Chapter 7
Property Measurements of Molten Oxides at High Temperature Using Containerless Methods

Takehiko Ishikawa, Paul-François Paradis, and Atsunobu Masuno

Abstract To understand the hyperordered structures found in new glasses fabricated with containerless methods, it is of paramount importance to know not only their atomic structures but also their macroscopic thermophysical properties. However, due to their high melting temperatures and the risk of contamination from the crucibles, molten oxides whose melting temperatures are above 2000 °C can hardly be processed using conventional methods. This explains that the published data on thermophysical properties are very scarce. In this chapter, four containerless methods capable of measuring several thermophysical properties such as density, surface tension, and viscosity are introduced. Three of them use a gas flow to levitate samples against gravity, while the electrostatic levitation furnace onboard the International Space Station utilizes the Coulomb force to spatially position samples in microgravity. Features of each method are summarized in this chapter, including their advantages and disadvantages. Finally, the measured data of refractory oxides whose melting temperatures are above 2000 °C are summarized.

Keywords Levitation · High temperature melts · Density · Viscosity

T. Ishikawa (✉)
Japan Aerospace Exploration Agency, Tsukuba 305-8505, Japan
e-mail: Ishikawa.takehiko@jaxa.jp

P.-F. Paradis
INO, Quebec G1P 4S4, Canada
e-mail: paul-francois.paradis@ino.ca

A. Masuno
Kyoto University, Kyoto 615-8520, Japan
e-mail: masuno.atsunobu.3k@kyoto-u.ac.jp

K. Hayashi (ed.), *Hyperordered Structures in Materials*, The Materials Research Society Series, https://doi.org/10.1007/978-981-99-5235-9_7

7.1 Introduction

Importance of levitation techniques is increasing in the research area of oxide glasses since new glasses fabricated with containerless methods exhibit structures that are significantly different from those of conventional glasses. They do not contain the corner-sharing tetrahedral networks which are commonly found in the conventional glasses [1]. Moreover, the new glasses show superior mechanical [2–6], optical [7–20], and magneto-optical properties [21, 22]. They are fabricated from the deeply undercooled melts with levitation techniques. To clarify the vitrification processes, the atomic structures of their liquidus phases as well as glass phases at high temperature are measured by combining the levitators with synchrotron X-ray and neutron diffraction [23–50], X-ray absorption fine structure (XAFS) [51–54], Raman scattering [55], and nuclear magnetic resonance (NMR) [56–60]. Detailed methods and procedures to obtain atomic structures from the measurements are described elsewhere in this book.

Macroscopic thermophysical properties of oxide melts are also important to understand the vitrification mechanism and phase selection processes from deeply undercooled melts. They are also inevitable to conduct MD simulations to obtain atomic structures and explore "hyperordered structures" in disordered atomic structure. For example, density data are necessary to calculate the total pair distribution function $G(r)$ from the measured total structure factor $S(Q)$ by X-ray or neutron diffraction experiments. As highlighted by Angell [47], a fundamental knowledge of both strong and fragile liquids (respectively high and low-glass-forming ability) can be inferred from the temperature dependence of viscosity. The heat capacities can be estimated thorough statistical/quantum mechanics once the binding energies between atoms are determined.

Such thermophysical properties as density, surface tension, viscosity, and heat capacity are usually measured using conventional methods with containers. However, to obtain accurate data without contamination from the crucibles, levitation methods are required for refractory oxide melts, in which melting temperatures are above 2000 °C.

In this chapter, methods to measure thermophysical properties of molten oxides with containerless processing (levitation) are presented and the data found in the literature summarized.

7.2 Methods for Containerless Processing with Oxide Samples

Four levitation methods used for oxide melts, namely the aerodynamic, the aero-acoustic, the gas film, and the electrostatic techniques are briefly described in this section. The electromagnetic levitation method (EML) used for metal/alloys [61–64]

is not applicable for oxide samples due to their poor electrical conductivities. Similarly, the acoustic levitation method [65, 66] is not suitable for high-temperature melt because it is very difficult to maintain a stable standing wave at high temperatures.

7.2.1 Aerodynamic Levitation

Aerodynamic levitation (ADL) is one of the simplest methods among the levitation methods. A sample can be stably levitated in a conical nozzle where a gas flow creates a stable point (pressure minimum) [67–69]. High power lasers are used to heat and melt the levitated samples. The typical sample size is around 1–3 mm in diameter and the molten sample is nearly spherical. By controlling the gas flow rate, steady sample levitation can be achieved.

Because of its simplicity, ADLs are widely used to produce spherical samples. Moreover, they are used for research on metastable phase formation from undercooled melts and fabrication of novel glasses which cannot be achieved with conventional methods using containers [2–22].

Originally, the nozzle used was so deep that heating, temperature measurement, and observation of the sample was possible only from the top. In the late 1990s, shallow nozzles were developed for the sake of synchrotron x-ray measurements on aerodynamically levitated liquid, which enabled the sample observation from the side [70]. Even if shallow nozzles were implemented, a full view of the sample is still not possible since the south pole of the sample is obstructed by the levitator. Furthermore, the lower part of the specimen is cooled by the flowing gas which introduces a large gradient in temperature. This issue can be alleviated by directing a second beam through the throat of the levitator. Care shall be taken to ensure that the levitator is leveled and that the laser beams hit the sample head-on. Not doing this would induce a rotation of the sample [71].

A typical setup for thermophysical property measurements with an ADL is shown in Fig. 7.1 [72]. To reduce the temperature gradient, a heating laser beam is divided to heat the aerodynamically levitated sample from the top and the bottom. A surface oscillation excitation system [73] induces an oscillatory pressure fluctuation on the gas flow and excites drop oscillation on the liquid sample. Detailed sample images are taken from a high-speed camera observing from the side with a proper backlight. Such experimental arrangement makes possible the determination of such thermophysical properties as density, surface tension, and viscosity of oxides in their liquid phases [73].

Coupled with X-ray/neutron diffraction facilities [47, 50, 70] and NMR [56–60], aerodynamic levitators were utilized to probe the atomic structure and dynamics of liquids at elevated temperatures. Furthermore, splitable nozzles [71] were successfully utilized in splat-quenching research [74, 75], drop calorimetry [76], and surface tension determination with innovative techniques (namely, droplet impingement [77] and bouncing [78]).

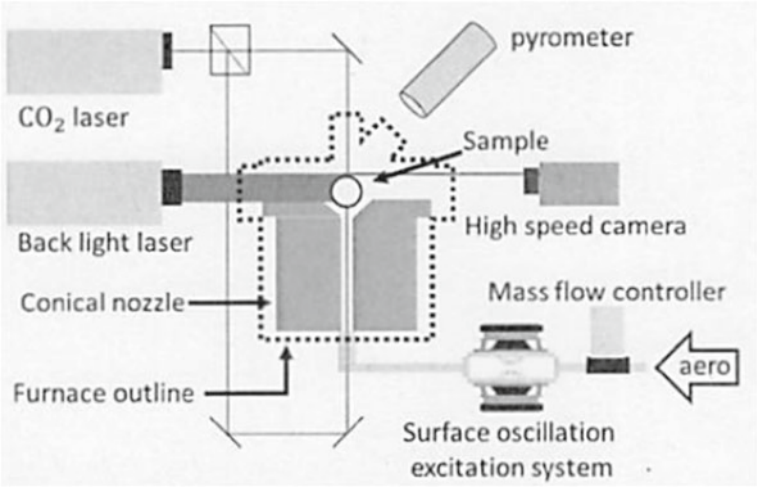

Fig. 7.1 Schematic of an aerodynamic levitation system for measuring thermophysical properties of molten oxides. Reproduced with permission from Ref. [72]

7.2.2 Aero-Acoustic Levitation

The aero-acoustic levitation (AAL) method first levitates a sample at an unstable location in the gas flow and stabilizes it through acoustic forces with surrounding transducers [79–81] (Fig. 7.2). A feedback control, based on the specimen position coordinates, is utilized to ensure adequate acoustic forces from the transducers allowing levitation of spheroids with diameters varying from about 1 to 3 mm. Upon melting, the strong acoustic pressure will make the sample to adopt an oblate-spheroid shape according to mass and surface tension. Full visibility of the sample is available. AALs combined with high-speed cameras were used for studies on metastable phase formation from undercooled oxide melts [82–94].

Developments on thermophysical property measurements have been conducted by Ushakov et al. since the 2010s. The authors were able to determine the density of a non-symmetric specimen through an image analysis [95]. This type of levitator was not used successfully so far for surface tension and viscosity measurements.

7.2.3 Gas Film Levitation

The gas film levitation method (GFL), mainly developed in France, floats a molten sample on a thin gas film formed between the sample and a pressurized porous diffuser (Fig. 7.3) [96]. Large samples (up to 10 g of copper, silver, and gold) can be levitated by this method. The molten sample is usually flat shaped, like that of sessile drop (SD) because of gravity. The bottom of the sample is hidden by a diffuser. Combined

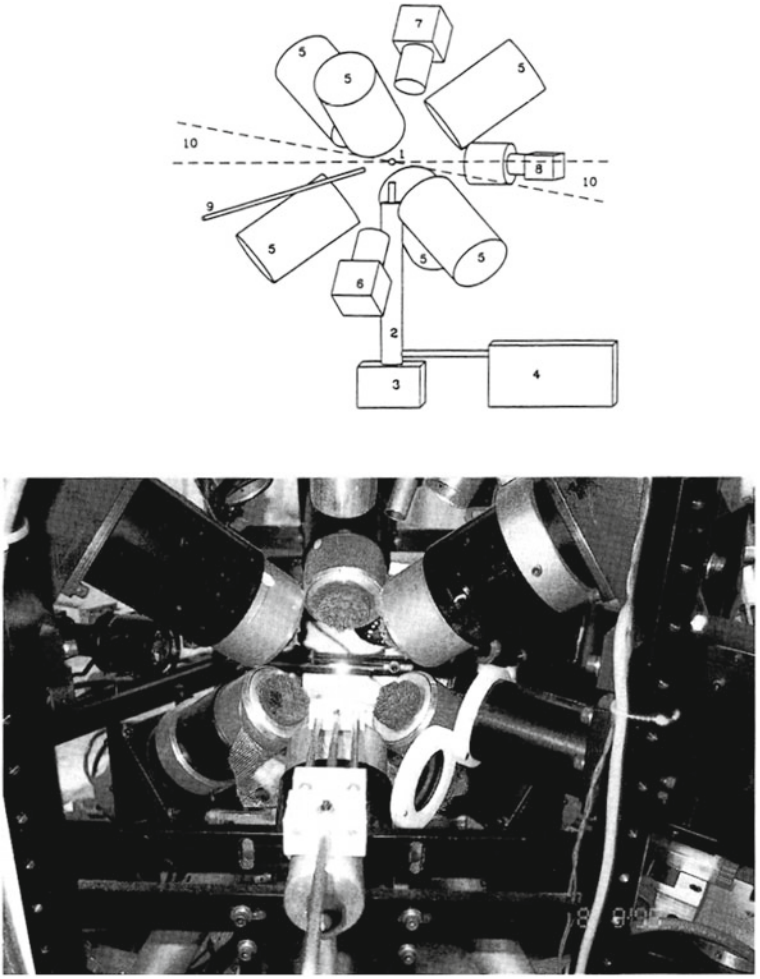

Fig. 7.2 Top: schematic diagram of an aero-acoustic levitation apparatus. 1, levitated sample; 2, gas flow tube and heater; 3, translation stage; 4, flow control system; 5, acoustic transduced (three-axis); 6, diode laser sample illuminator; 7, sample position detector (three-axis); 8, video camera; 9, vacuum chuck; 10, laser beam heating. Bottom: photograph of the aero-acoustic levitation apparatus showing a molten aluminum oxide sample at a temperature of 2700 K levitated in argon. Reproduced with permission from Ref. [81]

by such heating systems as a furnace or an electromagnetic heating, samples can be melted. Since the distance between the levitated sample and the lower diffuser is small (<100 μm), there is a risk for the hot sample to touch with the graphite diffuser, making its operation very challenging. This technique was used first for oxides and metallic glass-forming melts, which melting temperatures were relatively low [96,

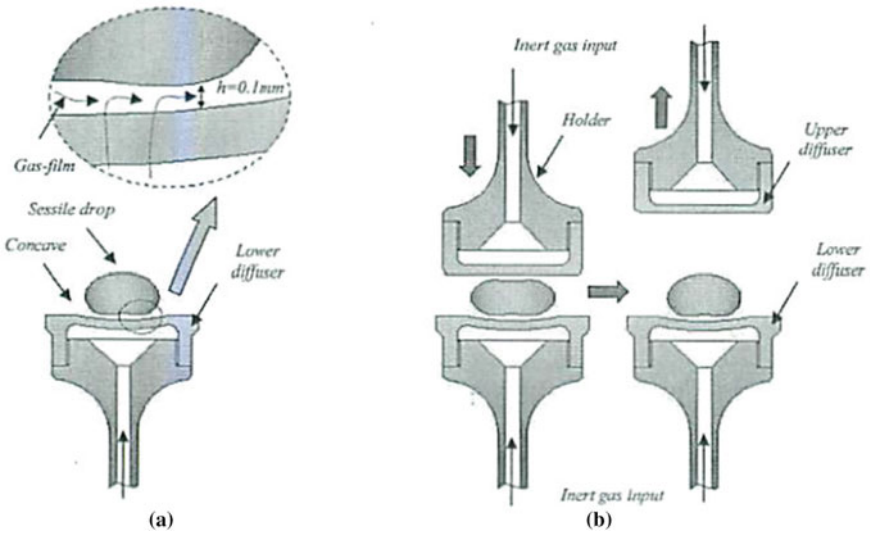

Fig. 7.3 Principles of the gas film levitation (**a**) and viscosity measurement (**b**). Reproduced with permission from Ref. [98]

97]. Later, the technique was also used to measure the thermophysical properties of the ZrO_2-Al_2O_3 system over the 1700–2350 °C temperature interval [98].

7.2.4 Electrostatic Levitation

The methods enumerated in the previous sections all have inconvenience with regard to the flowing gas which induces deformation, rotation/precession, thermal gradient, and internal flow in or on the levitated specimen [99]. For one, the rotation/precession of the sample makes the experimental uncertainty larger on image-based volume calculation. Moreover, the internal flow in the molten sample may produce huge uncertainties on viscosity measurements. It has been reported that the viscosity of molten metals measured with electromagnetic levitators in microgravity is more than twice as high as the literature values due to the internal flow [100, 101]. Although the effects of internal flow on viscosity measurements with ADL and GFL have not been well studied, careful consideration shall be given based on these observations.

A Coulomb force between a charged sample and surrounding electrodes is utilized in the electrostatic levitation method (ESL) to levitate against gravity. In order to stably levitate a sample, a high-speed feedback control system is required, and therefore, the levitation system is more complicated than other levitation system. A full view of the sample (around 1–3 mm in diameter) can be obtained. Figure 7.4 shows a schematic diagram of the sample position control system in ESL [102]. A charged sample can be levitated between the two disk electrodes (top and bottom electrodes),

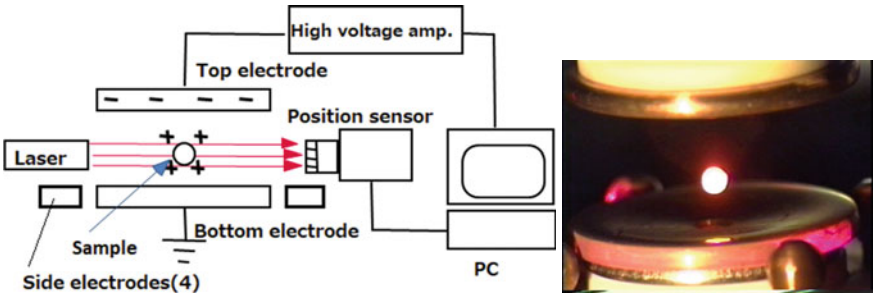

Fig. 7.4 Schematic diagram of the electrode configuration and active position control system used in the JPL high temperature electrostatic levitator

which are parallel and separated by about 10 mm. A collimated laser beam projects the sample's shadow onto a position sensor and its position is measured. The position data is sent to a computer where a PID (Proportional-Integral–Differential) feedback control algorithm determines the voltage to stabilize the sample position. The control voltage is amplified and finally sent to the top electrode. In addition, four small electrodes around the bottom electrode are used to control the horizontal sample position. Optical devices such as pyrometers, heating lasers, and observation cameras are aligned in the horizontal plane between the top and bottom electrodes. Since the original development by Rhim et al. [102], almost all ground-based facilities have employed this control system [103, 104].

Since there is no gas flow, a levitated sample is nearly spherical in its liquid state. The internal flow is very small. The ESL method is widely used for metals and alloys with high vacuum environments on the ground. Methods to determine density [105], surface tension, viscosity [106], and heat capacity [107] have been developed and these properties have been measured on variety of refractory metals and alloys [104]. Moreover, some electrostatic levitators have been designed to be combined with X-ray and neutron diffraction facilities [108–112].

Electrostatic levitation can, in principle, be used with a variety of specimens. Having said that, oxide compositions are difficult to process under terrestrial gravitational condition (1-g) because: (1) it is challenging to accumulate enough electrical charges (about 10^{-10} C); (2) a gas atmosphere is needed to avoid de-oxidization and evaporation of such materials. However, the electric field necessary to levitate a sample against gravity (10–20 kV/cm) cannot be applied in gaseous environments because electric discharges occur easily among electrodes. For these reasons, only a few materials (namely $BaTiO_3$, $Y_3Al_5O_{12}$, Nd-$CaAl_2O_{15}$, Al_2O_3, and $BiFeO_3$) have been levitated and melted on the ground [113–116].

Under the microgravity conditions offered by the ISS (10^{-6}-g), such a large electric field is not required for the sample positioning. Therefore, the above-mentioned restrictions are drastically alleviated. Firstly, oxide samples with much fewer electrical charges can be levitated. Samples with surface charges as low as 10^{-13} C can be levitated using ±2 kV/cm electric field. Secondly, levitation experiments

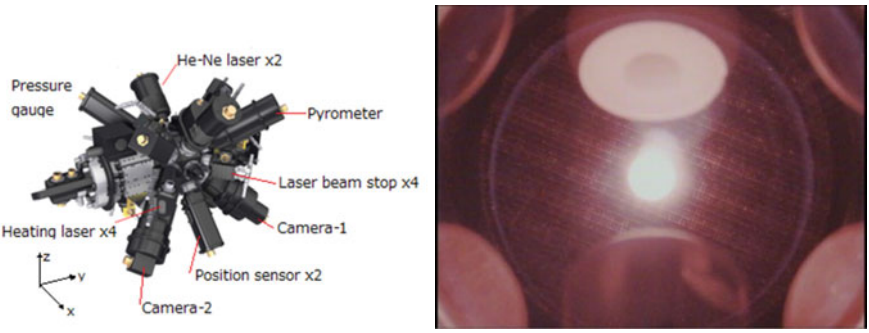

Fig. 7.5 Drawing of the processing chamber in the ISS-ELF (left) and a molten sample levitated between electrodes in the ISS-ELF (right)

in gaseous environments become possible without the electric discharges between electrodes. Moreover, the molten sample becomes perfectly spherical and internal natural convection is strongly suppressed. The microgravity offered by the International Space Station (ISS) is therefore an ideal environment for high temperature oxide melts with electrostatic levitation method.

Because of these merits, the Japan Aerospace Exploration Agency (JAXA) has developed an electrostatic levitation furnace onboard the ISS (ISS-ELF) and it has been operational since 2016 (Fig. 7.5). Detailed descriptions on the facility and status of thermophysical property measurements with it are found elsewhere [117]. The ISS-ELF can measure density, surface tension, and viscosity of oxide melts at high temperatures. A similar facility has been developed and installed in the Chinese Space Station since 2021 [118].

7.3 Thermophysical Property Measurements of Refractory Oxide Melts Using Containerless Methods

7.3.1 Density

With the sample mass (m) and its volume (V), density (r) of the sample can be obtained by,

$$\rho = m/V. \tag{7.1}$$

Therefore, the density can be calculated by volume measurements of the levitated samples. They are obtained from sample images with the assumption that the molten samples are axisymmetric. Sample images used for volume measurements

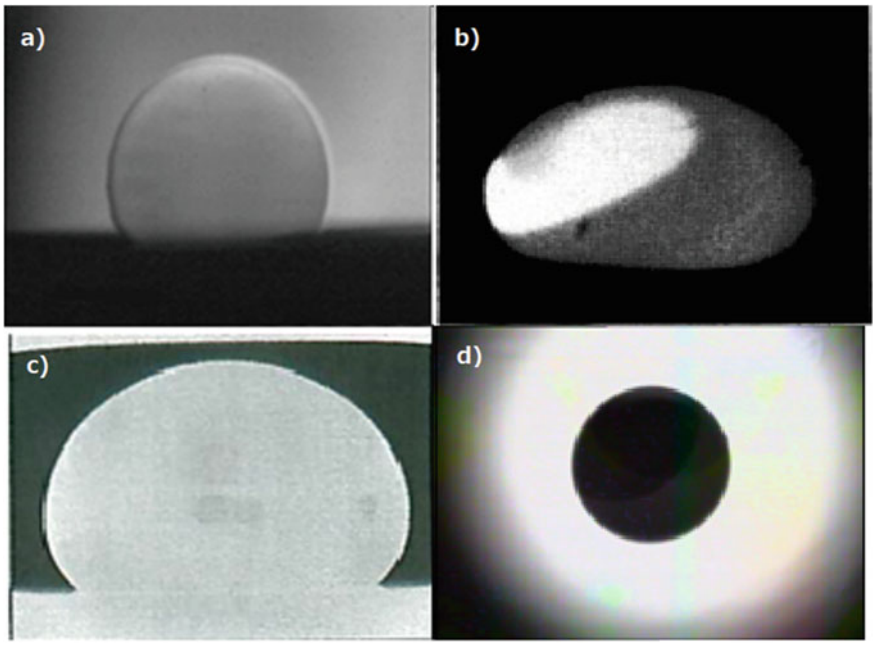

Fig. 7.6 Magnified sample images viewing from horizontal axis; **a** ADL, **b** AAL (reproduced with permission from Ref. [81]), **c** GFL (reproduced with permission from Ref. [98]), and **d** ESL

in each levitation method are summarized in Fig. 7.6. Since all images are vertically axisymmetric, the sample images should be taken from horizontal plane.

As for the earlier versions of ADL, the conical nozzle was so deep that it fully hid the sample, which prevented the observation from the side. Sample observation was done from the top, which was parallel to the symmetric axis, and led to erroneous volume measurements. In recent setups, shallow nozzles were developed allowing sample observation from the side.

Control of rotation axis is also important. With the ADL, samples are easily rotated about the horizontal axis by strong gas flows. Besides, photon pressure from high power lasers induces a rotation torque on the samples [119]. Uncontrolled sample rotation introduces substantial errors. Le Maux et al. installed a needle horizontally beside the conical nozzle in their ADL system. A thin gas jet is blown through the needle to rotate the levitated sample around the vertical axis [120]. A rotation control mechanism using the principle of induction motor is applied to some ESLs to intentionally spin the sample and stabilize its rotation axis [121]. This method is not applicable for insulators (oxide samples). In the ISS-ELF, any sample rotation is suppressed by the surrounding pressurized gas. A method to precisely measure the volume from an ellipsoid with random axis has been reported [122]. However, at least one additional camera is required to reconstruct the three-dimensional sample shape.

The computer-based image analyses detect the edge of the sample. A good contrast between the sample and the background is important to accurately determine the volume. At high temperatures, the sample irradiance is very large in the infrared portion of the spectrum, which blurs the sample contour. The Ultra-Violet (UV) background (taking images in the 380 nm (UV) to 530 nm (green) wavelength range) can minimize this error, because the sample irradiance is less pronounced in this part of the spectrum [123].

In our image analysis with the ESL [105], 400 edge points are detected from a sample image and converted to polar coordinates (R, θ). Then, these points are fit with the spherical harmonic functions through sixth order as

$$R(\theta) = \sum_{n=0}^{6} c_n P_n(\cos\theta) \tag{7.2}$$

where $P_n(\cos\theta)$ is the n-th order Legendre polynomials and c_n are the coefficients which are determined to minimize the following value

$$F = \sum_{j=0}^{400} \left\{ R_j - R_j(\theta) \right\}^2 \tag{7.3}$$

Then, the volume is calculated by

$$V = \frac{2\pi}{3} \int_0^{\pi} R^3(\theta) \sin\theta d\theta \tag{7.4}$$

Similar image analyses are carried out for all levitation methods (namely ADL, AAL, and GFL) volume calculations.

The measured density values of molten Al_2O_3 and their temperature dependence found in literature are shown in Fig. 7.7 and in Table 7.1. Al_2O_3 is a suitable material to evaluate the measurement methods since a relatively large number of data were taken on this material.

It is clearly seen that the density data obtained at the melting temperature (r_m) by containerless methods (ESL, ADL, and GFL), displayed in warm colors (Fig. 7.7), yielded a better agreement than those of conventional techniques (Sessile drop (SD), Pendant drop (PD), Maximum bubble pressure (MBP), and Archimedean [128–137]). Furthermore, the temperature coefficients ($\mathrm{d}\rho/\mathrm{d}T$) obtained with conventional techniques are greater than those for containerless ones. Contamination from the crucibles may lead to the smaller density values at high temperature.

For containerless techniques, discrepancies are very little. Data obtained with non-optimal setups (observation from above for ADL and observing without UV background) led to smaller density data and steeper temperature gradients. Even

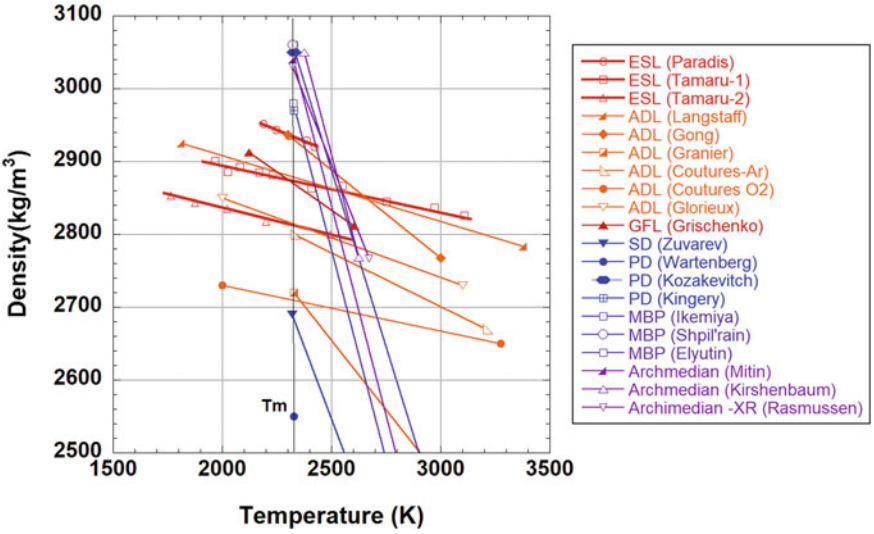

Fig. 7.7 Measured Density of molten Al_2O_3 as a function of temperature. Lines in bright color (red, orange, and pink) are data obtained by containerless methods, while lines in cold (blue, violet, and purple) are by conventional method

though part of the specimen is hidden in the ADL setups, the errors introduced on the volume estimation are negligibly small for Al_2O_3.

Melting temperatures of lanthanoid sesquioxides, ZrO_2, and HfO_2 are above 2400 °C, which is more than 250 K higher than that of Al_2O_3. Therefore, it is very hard to melt and measure properties on these specimens with conventional techniques. Literature values are very rare and most of the reported data have been measured by containerless methods. Measured density data of these oxides are listed in Table 7.2. The properties of Ln_2O_3 (Ln = Gd, Tb, Ho, Er, Tm, Yb, Lu) have been systematically determined with the ISS-ELF [138–140] and, using the structural analysis data obtained with X-ray and neutron facilities, the atomic structure of the molten phase was revealed for Er_2O_3 (non-glass forming liquid) [25]. So far, ZrO_2 and HfO_2 compositions were not successfully processed in the ISS-ELF. However, two density data sets were obtained for ZrO_2 with aerodynamic levitation and they agree well within the experimental uncertainty [24, 143]. For HfO_2, only one series of experiments was achieved with the aero-acoustic levitator [95]. Because experimental data are scarce, comparison is done with the estimated values from molecular dynamics (MD) calculations [142, 144, 145] (see Table 7.2).

Table 7.1 Density of molten Al_2O_3

ρ_m (10^3 kg m^{-3})	dρ/dT (kg m^{-3} K^{-1})	Temperature (K)	References
2.93	−0.12	2175–2435	ESL [116]
2.87	−0.064	1913–3139	ESL [117]
2.81	−0.074	1732–2597	ESL [117]
2.9	−0.09	1900–3240	ADL [73]
2.93	−0.242	2300–3000	ADL [124]
2.79	−0.117	2000–3100	ADL [125]
2.71	−0.0678	2000–3275	ADL [126]
2.80	−0.151	2327–3210	ADL [126]
2.72	−0.28	2323–2965	ADL [127]
2.87	−0.2098	2123–2603	GFL [98]
2.69	−0.79	2320–3100	SD [128]
2.55		2327	PD [129]
3.05		2327	PD [130]
2.97		2327	PD [131]
3.06		2327	MBP [132]
3.06	−0.965	2323–3023	MBP [133]
2.98	−1.15	2325–2775	MBP [134]
3.04	−1.15	2323–2828	Archimedean [135]
3.05	−1.127	2375–2625	Archimedean [136]
3.03	−0.752	2323–2673	Archimedean + X-radiograph [137]

7.3.2 Surface Tension and Viscosity

Drop oscillation method is used to simultaneously measure surface tensions and viscosities of levitated melts for both ADL and ESL. Detailed measurement procedures are described by Rhim et al. [105] for ESL and by Langstaff et al. [72] for ADL. This technique initially induces "mode-2" sample oscillations (depicted in Fig. 7.8a) on a drop. Once there is no more excitation, the deformation of the sample gradually reduces due to viscosity. The change in the sample oscillation is recorded (Fig. 7.8b) allowing to find surface tension and viscosity by calculation. The characteristic oscillation frequency f_2 can be obtained using FFT (Fast Fourier Transform) analysis, whereas the damping constant τ_2 can be determined from the time-fluctuation curve. The surface tension γ and viscosity η can be found using [144, 145],

$$\gamma = \frac{\rho r_0^3 (2\pi f_2)^2}{8}, \tag{7.5}$$

and

Table 7.2 Density of oxide melts which melting temperatures are above 2400 °C

Samples	T_m (K)	ρ_m (kgm^{-3})	$d\rho/dT$ ($kg\ m^{-3}\ K^{-1}$)	Remarks
Y_2O_3	2704	4600 ± 150		AAL [95]
		4420	−0.8927 ± 0.222	ADL [138]
Gd_2O_3	2693	7268 ± 205		ESL [139, 140]
		6947 ± 340	−1.048 ± 0.112	ADL [138]
Tb_2O_3	2683	7451 ± 112		ESL [140]
Ho_2O_3	2685	8035 ± 108		ESL [140]
Er_2O_3	2686	8170 ± 245		ESL [140]
		7573 ± 530	−0.3273 ± 0.179	ADL [138]
Tm_2O_3	2698	8304 ± 148	−0.18 ± 0.05	ESL [141]
Yb_2O_3	2708	8425 ± 217	−0.55 ± 0.08	ESL [141]
	2708	7940	−0.74 ± 0.13	ADL [138]
	2708	8400 ± 200		AAL [95]
	2707	8750	(−3.9)	MD [142]
Lu_2O_3	2763	8627 ± 240	−0.43 ± 0.08	ESL [141]
ZrO_2	2983	5048	−0.89	ADL [24]
	2983	4690		ADL [143]
	2983	4740–4860	(−0.44)	MD [144]
HfO_2	3073	8200 ± 300		AAL [95]
		8530–8730	(−0.7)	MD [144]
		8160		MD [145]

$$\eta = \frac{\rho r_0^2}{5\tau_2} \tag{7.6}$$

where r_0 is the radius of the drop, and ρ is the density of the sample.

In the case of ESL, an excitation of sample oscillation is done by adding a sinusoidal excitation voltage on the levitation electric field. When the frequency of the sinusoidal input matches the characteristic oscillation frequency (f_2), the sample exhibits a large deformation due to resonance. A pair of loudspeakers is inserted in the gas line in the ADL and a forced oscillation is done by pulsing a gas stream by the speakers [73].

Measurement of the sample oscillation is done by two methods. The first method utilizes a high-speed camera. It records hundreds of images of sample oscillation within a second. These images are analyzed in a similar manner as those for density measurements to obtain the geometries of the sample. By analyzing the fluctuation of the sample diameters as a function of time, f_2 and τ_2 can be obtained. This method can visually ensure that mode-2 oscillation was excited. However, it requires to analyze more than 100 still images to get a time-diameter profile and this is very

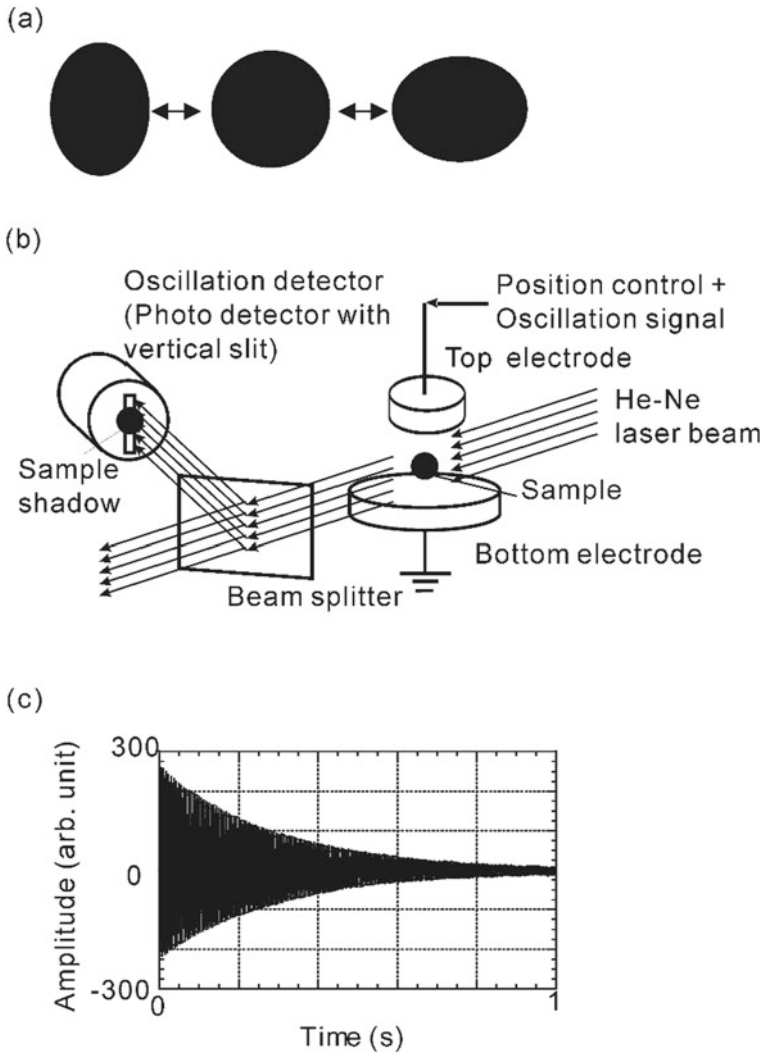

Fig. 7.8 **a** Sketch of mode-2 oscillation, **b** Sketch of the setup for specimen excitation and oscillation detection in the ESL and **c** representative data obtained with the oscillation detector. Reproduced with permission from Ref. [103]

time consuming. In another method, a power meter is used. A collimated laser beam projects a sample shadow on the power meter covered with a slit [103, 106] as shown in Fig. 7.8c. The sample deformation is then detected as a fluctuation of the laser power onto the power meter. This method is simple and can quickly help estimate f_2 and τ_2. It is hard to tell if mode-2 is properly excited. Driven by cost effectiveness and stringent limitations on available power, a power meter was chosen for the ISS-ELF.

The surface tension can be determined from the drop shape in GFL, like that used for the SD method. In GFL, viscosity can be measured by two different modes, periodic and aperiodic. The periodic mode method is similar to the oscillation drop method and suitable for low viscosity melts. In aperiodic mode, the upper diffuser (shown in Fig. 7.3b), is used to make a large deformation on the highly viscous materials (over 1 Pa s) to measure the viscosity [96–99]. Two new techniques in ADLs using splitable nozzles have been developed to measure surface tension. In the first method, named the drop impingement method, a levitated sample is dropped from the nozzle and impinges on a plate. The change of the surface energy during impingement is calculated with the detailed analysis of the sample shapes recorded by a high-speed camera allowing the surface tension to be evaluated [77]. The second method, called drop-bounce method, is similar to the drop oscillation method. By dropping and bouncing the molten sample on a plate, a mode 2 oscillation with a certain amplitude can be induced to the sample, from which surface tension and viscosity can be obtained [78]. The main demerit of these methods with the splitable nozzle is the temperature measurement. Currently it is very hard to accurately measure the sample temperature when it falls and bounces. However, these methods will be useful for the samples of molten materials under high vapor pressures with which stable levitation is very hard due to evaporation.

The surface tension values of molten Al_2O_3 measured by containerless methods as well as conventional methods found in the literature are depicted in Fig. 7.9 and listed in Table 7.3.

For the surface tension determined at the melting temperature (γ_m), all values obtained by containerless methods (ESL, ADL, and GFL [73, 77, 78, 98, 148–150]) shown in bright colors (Fig. 7.9), agree well within their experimental uncertainties. However, some of the data obtained by ADLs show positive temperature dependence. This could originate from the excitation of non-axisymmetric mode-2 oscillations. The temperature dependency of GFL also displays a positive dependence [98]. When measured by conventional techniques (cold colors), surface tension exhibits greater and steeper temperature dependencies. These results could be attributable to reactions between the specimens and the containers. Because containers were not utilized with the PD technique [131, 151, 152], the obtained data agree well. However, only γ_m can be determined with this technique.

The measured surface tension data of oxide melts, whose melting temperatures are above 2400 °C, are listed in Table 7.4. The number of measured data is less than that of density. It is because a more stable sample position control is required for the oscillation drop experiment. Up to now, the surface tension of Tb_2O_3 was measured with the ISS-ELF [149]. The surface tension of ZrO_2 was measured by the ADL and reported in [157].

The viscosity of molten Al_2O_3 and its temperature dependence found in the literature are listed in Table 7.5 as well as shown in Fig. 7.10. The measured viscosities at the melting temperature (η_m) by containerless methods (ESL, GFL, and ADL) show better agreement than those by conventional methods (rotating cup [158, 159] and oscillating cup [160, 161]). However, η_m obtained by ADLs show higher values than those reported by ESL (higher than the experimental uncertainty of 30%). This

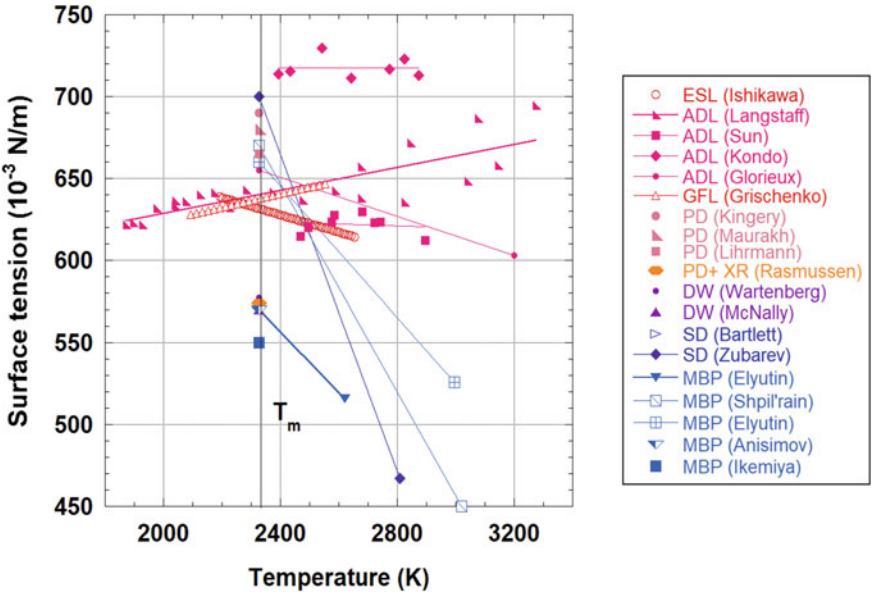

Fig. 7.9 Measured surface tension of molten Al_2O_3 as a function of temperature. Lines in bright colors (red, orange, and pink) are data from containerless methods, including pendant drop (PD), while lines in cold colors (blue, violet, and purple) are from conventional methods

discrepancy may be caused by the sample internal flow in the ADL. It was reported that the viscosities measured with an EML in the ISS were up to 2–8 times higher than the literature values, due to the internal flow [100, 101]. The gas flow around the sample in ADL may introduce a flow inside the sample and may impact the viscosity measurements.

In general, the viscosity data of oxide materials are very scarce. The measured viscosity data of some oxides with which the melting temperatures are above 2400 °C are listed in Table 7.6. So far, the viscosity of Tb_2O_3 was measured with the ISS-ELF [149]. In addition, the viscosity of ZrO_2 was measured with ADL [143].

Recently, MD simulations were conducted to estimate the viscosity. Structural data were obtained using high-energy x-ray diffraction experiments combined with the ADLs and used for calculations. The calculated viscosity of Er_2O_3 was 3 mPa s, which is 1/10 of the viscosity of Tb_2O_3. The viscosity of ZrO_2 was calculated to be around 5 mPa s [44] which is 60% smaller than the measured value.

There is a large discrepancy between the experimental and the calculated data. More efforts are necessary on both sides. On the measurement side, ADLs will be powerful tools to measure viscosities of high temperature melts if the effects of the internal flow induced by the gas flow are properly evaluated. For the ISS-ELF, improvement of the position control is required. For MD calculations, viscosity data are estimated from diffusivity using Stokes–Einstein relation. The applicability of this relation should be verified.

Table 7.3 Surface tension of molten Al_2O_3

γ_m (10^{-3}N m^{-1})	dγ/dT (10^{-3}N m^{-1} K^{-1})	Temperature (K)	References
632	-5.3×10^{-2}	2193–2653	ESL [148, 149]
650	-3.9×10^{-2}	2327–3200	ADL [150]
~640	(3.5×10^{-2})	(1870–3275)	ADL [73]
~623	(-5.9×10^{-3})	(2468–2896)	ADL + Drop bounce [78]
~717	~ 0	(2393–2872)	ADL + Drop impingement [77]
638	*	2123–2603	GFL [98]
690	–	2327	PD [131]
680	–	2327	PD [151]
665	–	2327	PD [152]
551	–	2327	SD [153]
700	-4.8×10^{-1}	2327–2810	SD [128]
570	–	2327	DW [154]
577	–	2327	DW [129]
550	–	2327	MBP [132]
570	-1.8×10^{-1}	2327–2620	MBP [155]
670	-3.2×10^{-1}	2327–3020	MBP [133]
660	-2.0×10^{-1}	2327–2995	MBP [134]
570	–	2327	MBP [156]
574	–	2327	PD + X-radiograph [137]

DW Drop weight
*$\gamma\ (T) = 517.286 + 7.658 \times 10^{-2}\ T\text{-}8.7 \times 10^{-6} T^2$

Table 7.4 Surface tension of oxide melts which melting temperatures are above 2400 °C

Samples	T_m (K)	γ_m (10^{-3} N m^{-1})	dγ/dT (10^{-3}N m^{-1} K^{-1})	Remarks
Tb_2O_3	2683	733.4	−0.039	ESL [149]
ZrO_2	2988	910 ± 10	−0.133 ± 0.116	ADL [157]

The drop oscillation technique can be used with materials having viscosity ranging from about 1 to 30 mPa s. For higher viscosity materials, oscillations damp too quickly and τ_2 cannot be determined accurately. Furthermore, if the viscosity is near 1 Pa s, the drop oscillation method cannot be implemented because a significant and periodic oscillation does not occur. Since, the oxide glass research asks for data over wide viscosity spans (1 mPa s to over 10 Pa s), the development of an aperiodic mode measurement is desired for both the aerodynamic (nozzle-type and gas-film) and electrostatic levitators.

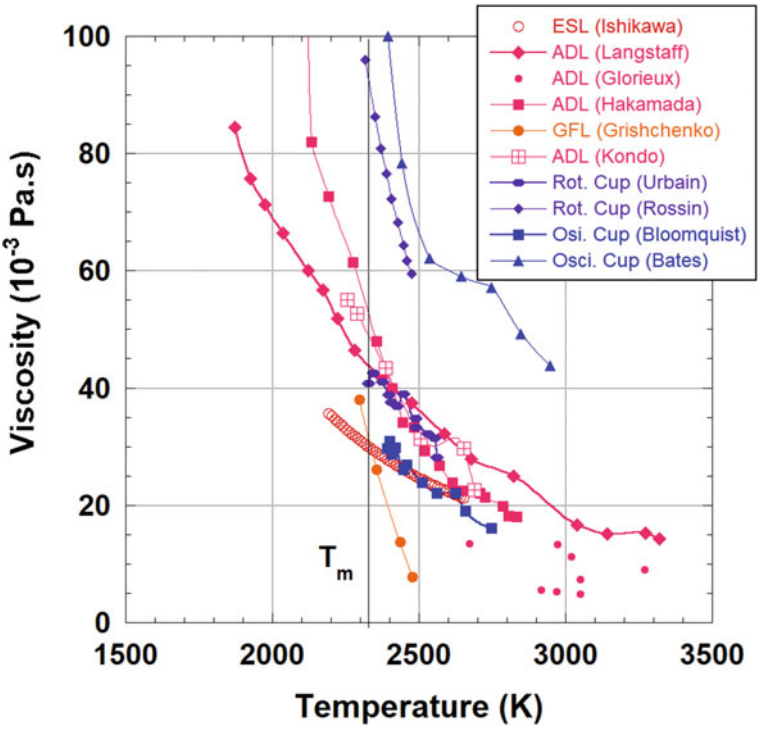

Fig. 7.10 Measured viscosity of molten Al_2O_3 as a function of temperature. Lines in bright colors (red, orange, and pink) are data from containerless methods, while lines in cold colors (blue, violet, and purple) are from conventional methods

Table 7.5 Viscosity of molten Al_2O_3 at its melting temperature

$\eta_m(10^{-3}$ Pa s)	References
30	ESL [148, 149]
45	ADL [73]
54	ADL [72]
50	ADL [143]
32	GFL [98]
135	Oscillating cup [158]
35	Oscillating cup [159]
~95	Rotating cup [160]
42	Rotating cup [161]

Table 7.6 Viscosity of oxide melts with melting temperatures above 2400 °C

Samples	T_m (K)	η_m (10^{-3} Pa s)	Temperature dependence[a]		Remarks
			η_0 (10^{-3} Pa s)	E (10^3 J/mol)	
Tb_2O_3	2683	26.3	0.33	97.6	ESL [149]
Er_2O_3	2693	3			MD [25]
ZrO_2	2988	13	0.96 ± 0.69	64 ± 20	ADL [143]
	2988	(5)			MD [44]

[a] $\eta(T)$ $\eta_0 \exp(E/RT)$, where R is the gas constant (8.31 J mol K^{-1})

7.3.3 Thermodynamic Properties

Since levitators are apparatuses to maintain molten samples at high temperatures, a variety of properties other than density, surface tension and viscosity can be obtained by combining with proper diagnostics methods. Thermodynamic properties such as constant pressure heat capacity (C_p), heat of fusion(ΔH_f), and enthalpy, can be determined with the containerless methods.

The heat of fusion of several refractory oxides is listed in Table 7.7. A drop calorimetry system combined with a splitable ADL (DnC; Drop and Catch method) has been developed to measure the enthalpy of a levitated sample [161]. This DnC set up potentially has the capability to measure the C_p.

Heat balance of a levitated sample is governed by

$$mC_p \frac{dT}{dt} = -\varepsilon_T \sigma_{SB} A\left(T^4 - T_w^4\right) - \kappa A(T - T_w) + Q \tag{7.7}$$

where, T_w is the temperature of the surrounding wall, ε_T is the total hemispherical emissivity of the sample, s_{SB} is the Stefan-Boltzmann constant, k is the overall heat transfer coefficient, A is the sample surface area, and Q is the laser power input. The first term (on the right side) is the contribution of radiation, and the second term is that of thermal conduction and convection. The second term can be zero under high vacuum environment, hence the ratio of the constant pressure heat capacity and hemispherical total emissivity (C_p/ε_T) can be calculated using the cooling curve (a time–temperature profile) where $Q = 0$ [106]. However, this method cannot be used in gaseous environment since the second term becomes too complicated as it needs to consider natural convection. Sun et al. [171] assumed that the heat dissipation in ADL is steady and can be calculated using Ranz-Marshall's equation [172]. Moreover, using two inert gases with different thermal conductivity values for levitation experiments, he calculated C_ps of several molten metals without ε_Ts. This technique will be used for the C_p measurements of refractory oxide melts with ADLs. C_ps of refractory oxide melts can also be estimated by MD calculations. Estimated values of ZrO_2 and HfO_2 are listed in Table 7.8.

Table 7.7 Measured heat of fusion of molten refractory oxides

Samples	T_m (K)	ΔH_f (kJ/mol)	Remarks
Al_2O_3	2327	109	ESL [116]
		107	Drop calorimetry [162]
		120 ± 20	DnC [76]
		118.4 ± 2.4	Drop calorimetry [163]
		107.9 ± 5.4	Drop calorimetry [164]
		89.5 ± 8.9	Thermal asset duration [76]
		107.5 ± 4.8	Drop calorimetry [165]
		113.0 ± 8.4	Evaluation [76]
		111.1 ± 4.2	Evaluation [76]
Y_2O_3	2712	119 ± 10	DnC [166]
La_2O_3	2578	78 ± 10	DTA [167, 168]
Nd_2O_3	2581	117 ± 10	DTA [169]
Yb_2O_3	2708	102 ± 10	DnC [170]
Lu_2O_3	2763	125 ± 10	DnC [170]
ZrO_2	2988	55 ± 7	DnC [144]
		54 ± 2	MD [144]
HfO_2	3073	61 ± 10	DnC [144]
		52 ± 2	MD [144]

DTA Differential Thermal Analysis

Table 7.8 Calculated heat capacity of molten refractory oxides

Samples	T_m (K)	C_p (J/molK)	
Al_2O_3	2327	153.5	ESL [116]
		184 ± 15	Drop carolimetry [162]
ZrO_2	2988	116 ± 25	MD [144]
		100	MD [173]
HfO_2	3073	109 ± 15	DnC [144]

7.3.4 Temperature Measurement

Temperature measurements with containerless processing are conducted by pyrometers. Therefore, precise values of samples' emissivity at measured wavelength are important. However, the emissivity data of refractory oxides are very scarce [95]. The emissivity of opaque sample can be estimated from its refraction index [80, 95]. However, absorption at the window should be considered if the pyrometer observes the sample through it. If the melting temperatures of a sample are known, the measured raw temperature values can be corrected to true temperature by matching the temperature plateau after recalescence to the given melting temperature, with the assumption that the emissivity of liquid phase is constant. This technique is

commonly used in containerless experiments with ADLs [174] and ESLs [116, 117, 148, 149]. In most cases, this temperature correction is reasonable. However, the sample temperatures will be underestimated, if the heat transfer by radiation may not allow sample reheating to the melting temperature by released heat of fusion, due to the relatively large surface to volume ratio and high temperatures [95]. Moreover, when the liquid sample vitrifies, there is no suitable landmark to correct the temperature.

Temperature measurement is a weak point of containerless processing. Many technical developments have been conducted to accurately measure the temperature of levitated samples, including in-situ emissivity determination using polarimetry [175, 176]. Currently, emissivity-free thermometry is under development and this technique will enable the temperature measurements without knowing the emissivity of the material [177].

7.4 Conclusions

This chapter described the status of thermophysical property measurements of molten refractory oxide materials using containerless processing methods. Measurements in microgravity conditions are ideal the since molten sample is perfectly spherical and free from internal flow. However, measurements in space are expensive and occasions are limited. Moreover, it is unclear if the facilities will be available after the ISS era. On the other hand, measurements with ADLs on the ground are cost-effective but need to establish the correction terms to cancel the error due to sample deformation, rotation, and internal flow. Our strategy is (1) to measure accurate thermophysical properties as much as possible with the ISS-ELF to obtain benchmark data, and (2) to establish correction terms theoretically using the knowledge of fluid dynamics, numerical simulations, and (3) to use the ADLs to experimentally confirm the correction terms on the ground. Since one of the most challenging issues is to accurately measure sample temperatures during containerless processing, further researches and developments along this axis are necessary and will be pursued.

Acknowledgements The authors would like to thank Dr. W.-K. Rhim for his extensive assistance throughout the development of the ISS-ELF. The authors also want to express their gratitude to the ISS crew members and ground operation staff for their support during the onboard assembly, check out, and experiments. It is also acknowledged that the ISS-ELF was designed and fabricated by the IHI Aerospace company. This work is supported by JSPS KEKENHI (Grant No. 20H05882 and 20H05878).

References

1. Masuno A (2022) J Phys Soc Jpn 91:091003
2. Rosales-Sosa GA, Masuno A, Higo Y, Inoue H, Yanaba Y, Mizoguchi T, Umada T, Okamura K, Kato K, Watanabe Y (2015) Sci Rep 5:15233
3. Rosales-Sosa GA, Masuno A, Higo Y, Watanabe Y, Inoue H (2018) J Am Ceram Soc 101:5030
4. Guo Y, Li J, Zhang Y, Feng S, Sun H (2021) iScience 24, 102735
5. Rosales-Sosa GA, Masuno A, Higo Y, Inoue H (2016) Sci Rep 6:23620
6. Ke X, Shan Z, Li Z, Tao Y, Yue Y, Tao H (2020) J Am Ceram Soc 103:3600
7. Arai Y, Itoh K, Kohara S, Yu J (2008) J Appl Phys 103:094905
8. Masuno A, Inoue H, Yu J, Arai Y (2010) J Appl Phys 108:063520
9. Masuno A, Inoue H (2010) Appl Phys Express 3:102601
10. Inoue H, Watanabe Y, Masuno A, Kanako M, Yu J (2011) Opt Mater 33:1853
11. Masuno A, Inoue H, Arai Y, Yu J, Watanabe Y (2011) J Mater Chem 21:17441
12. Masuno A, Watanabe Y, Inoue H, Arai Y, Yu J, Kaneko M (2012) Phys Status Solidi C 9:2424
13. Yoshimoto K, Masuno A, Inoue H, Watanabe Y (2012) J Am Ceram Soc 95:3501
14. Masuno A, Inoue H, Yoshimoto K, Watanabe Y (2014) Opt Mater Express 4:710
15. Yoshimoto K, Masuno A, Inoue H, Watanabe Y (2015) J Am Ceram Soc 98:402
16. Yoshimoto K, Masuno A, Ueda M, Inoue H, Yamamoto H, Kawashima T (2017) Sci Rep 7:45600
17. Yoshimoto K, Masuno A, Ueda M, Inoue H, Yamamoto H, Kawashima T (2018) J Am Ceram Soc 101:3328
18. Masuno A, Iwata T, Yanaba Y, Sasaki S, Inoue H, Watanabe Y (2019) Dalton Trans 48:10804
19. Chung J, Yanaba Y, Nakatsuka Y, Watanabe Y, Inoue H (2019) Int J Appl Glass Sci 10:181
20. Chung J, Watanabe Y, Yanaba Y, Nakatsuka Y, Inoue H (2020) J Am Ceram Soc 103:167
21. Suzuki F, Sato F, Oshita H, Yao S, Nakatsuka Y, Tanaka K (2018) Opt Mater 76:174
22. Suzuki F, Fujita N, Sato F (2019) Proc SPIE 10914:1091412
23. Benmore CJ, Weber JKR (2017) Adv Phys X 2:717
24. Kohara S, Akola J, Patrikeev L, Ropo M, Ohara K, Itou M, Fujiwara A, Yahiro J, Okada JT, Ishikawa T, Mizuno A, Masuno A, Watanabe Y, Usuki T (2014) Nat Commun 5:5892
25. Koyama C, Tahara S, Kohara S, Onodera Y, Småbråten DR, Selbach SM, Akola J, Ishikawa T, Masuno A, Mizuno A, Okada JT, Watanabe Y, Nakata Y, Ohara K, Tamaru H, Oda H, Obayashi I, Hiraoka Y, Sakata O (2020) NPG Asia Mater 12:43
26. Alderman OLG, Skinner LB, Benmore CJ, Tamalonis A, Weber JKR (2014) Phys Rev B 90:094204
27. Skinner LB, Barnes AC, Salmon PS, Hennet L, Fischer HE, Benmore CJ, Kohara S, Weber JKR, Bytchkov A, Wilding MC, Parise JB, Farmer TO, Pozdnyakova I, Tumber SK, Ohara K (2013) Phys Rev B 87:024201
28. Shi C, Alderman OLG, Berman D, Du J, Neuefeind J, Tamalonis A, Weber JKR, You J, Benmore CJ (2019) Front Mater 6:38
29. Mei Q, Benmore CJ, Weber JKR (2007) Phys Rev Lett 98:057802
30. Skinner LB, Benmore CJ, Weber JKR, Wilding MC, Tumber SK, Parise JB (2013) Phys Chem Chem Phys 15:8566
31. Skinner LB, Benmore CJ, Weber JKR, Williamson MA, Tamalonis A, Hebden A, Wiencek T, Alderman OLG, Guthrie M, Leibowitz L, Parise JB (2014) Science 346:984
32. Krishnan S, Felten JJ, Rix JE, Weber JKR, Nordine PC, Beno MA, Ansell S, Price DL (1997) Rev Sci Instrum 68:3512
33. Kohara S, Itou M, Suzuya K, Inamura Y, Sakurai Y, Ohishi Y, Takata M (2007) J Phys: Condens Matter 19:506101
34. Hennet L, Pozdnyakova I, Bytchkov A, Cristiglio V, Zanghi D, Brassamin S, Brun J-F, Leydier M, Price DL (2008) J Non-Cryst Solids 354:5104
35. McMillan PF (2008) Nat Mater 7:843

36. Hennet L, Cristiglio V, Kozaily J, Pozdnyakova I, Fischer HE, Bytchkov A, Drewitt JWE, Leydier M, Thiaudière D, Gruner S, Brassamin S, Zanghi D, Cuello GJ, Koza M, Magazù S, Greaves GN, Price DL (2011) Eur Phys J: Spec Top 196:151
37. Skinner LB, Benmore CJ, Weber JKR, Tumber S, Lazareva L, Neuefeind J, Santodonato L, Du J, Parise JB (2012) J Phys Chem B 116:13439
38. Skinner LB, Benmore CJ, Weber JKR, Du J, Neuefeind J, Tumber SK, Parise JB (2014) Phys Rev Lett 112:157801
39. Maram PS, Ushakov SV, Weber RJK, Benmore CJ, Navrotsky A (2015) J Am Ceram Soc 98:1292
40. Alderman OLG, Ferlat G, Baroni A, Salanne M, Micoulaut M, Benmore CJ, Lin A, Tamalonis A, Weber JKR (2015) J Phys: Condens Matter 27:455104
41. Weber JKR, Tamalonis A, Benmore CJ, Alderman OLG, Sendelbach S, Hebden A, Williamson MA (2016) Rev Sci Instrum 87:073902
42. Kohara S, Ohara K, Tajiri H, Song C, Sakata O, Usuki T, Benino Y, Mizuno A, Masuno A, Okada JT, Ishikawa T, Hosokawa S (2016) Z Phys Chem 230:339
43. Saito Y, Yonemura T, Masuno A, Inoue H, Ohara K, Kohara S (2016) J Ceram Soc Jpn 124:717
44. Alderman OLG, Benmore CJ, Weber JKR, Skinner LB, Tamalonis AJ, Sendelbach S, Hebden A, Williamson MA (2018) Sci Rep 8:2434
45. Alderman OLG, Benmore CJ, Neuefeind J, Coillet E, Mermet A, Martinez V, Tamalonis A, Weber R (2018) Phys Rev Mater 2:043602
46. Alderman OLG, Benmore CJ, Lin A, Tamalonis A, Weber JKR (2018) J Am Ceram Soc 101:3357
47. Kohara S, Ohara K, Ishikawa T, Tamaru H, Weber R (2018) Quantum Beam Sci 2:5
48. Alderman OLG, Benmore CJ, Feller S, Kamitsos EI, Simandiras ED, Liakos DG, Jesuit M, Boyd M, Packard M, Weber R (2020) J Phys Chem Lett 11:427
49. Shi C, Alderman OLG, Tamalonis A, Weber R, You J, Benmore CJ (2020) Commun Mater 1:80
50. Ohara K, Onodera Y, Kohara S, Koyama C, Masuno A, Mizuno A, Okada JT, Tahara S, Watanabe Y, Oda H, Nakata Y, Tamaru H, Ishikawa T, Sakata O (2020) Int J Microgravity Sci Appl 37:370202
51. Ohara K, Onodera Y, Murakami M, Kohara S (2021) J Phys: Condens Matter 33:383001
52. Alderman OLG, Benmore CJ, Tamalonis A, Sendelbach S, Heald S, Weber R (2016) J Phys Chem C 120:26974
53. Alderman OLG, Lazareva L, Wilding MC, Benmore CJ, Heald SM, Johnson CE, Johnson JA, Hah H-Y, Sendelbach S, Tamalonis A, Skinner LB, Parise JB, Weber JKR (2017) Geochim Cosmochim Acta 203:15
54. Landron C, Hennet L, Berthet P, Coutures J-P, Berar J-F (1999) Jpn J Appl Phys 38:87
55. Simon P, Moulin B, Buixaderas E, Raimboux N, Herault E, Chazallon B, Cattey H, Magneron N, Oswalt J, Hocrelle D (2003) J Raman Spectrosc 34:497
56. Côté B, Massiot D, Taulelle F, Coutures J-P (1992) Chem Geol 96:367
57. Florian P, Massiot D, Poe B, Farnan I, Coutures J-P (1995) Solid State Nucl Magn Reson 5:233
58. Massiot D, Trumeau D, Touzo B, Farnan I, Rifflet J-C, Douy A, Coutures J-P (1995) J Phys Chem 99:16455
59. Gruener G, Odier P, De Sousa Meneses D, Florian P, Richet P (2001) Phys Rev B 64, 024206
60. Massiot D, Fayon F, Montouillout V, Pellerin N, Hiet J, Roiland C, Florian P, Coutures J-P, Cormier L, Neuville DR (2008) J Non-Cryst Solids 354:249
61. Egry I (2000) High Temp High Press 32:127
62. Lohöfer G, Schneider S, Egry I (2001) Int J Thermophys 22:593
63. Luo Y, Damaschke B, Lohöfer G, Samwer K (2020) npj Microgravity 6, 10
64. Mohr M, Wunderlich R, Dong Y, Furrer D, Fecht H-J (2021) Adv Eng Mater 23:2001143
65. Wang TG, Anilkumar AV, Lee CP, Lin KC (1994) J Fluid Mech 276:389
66. Wang TG, Anilkumar AV, Lee CP (1996) J Fluid Mech 308:1
67. Oran WA, Berge LH (1982) Rev Sci Instrum 53:851

68. Nordine PC, Atkins RM (1982) Rev Sci Instrum 53:1456
69. Paradis P-F, Babin F, Gagné J-M (1996) Rev Sci Instrum 67:262
70. Weber R, Wilke SK, Benmore CJ (2022) J Phys Soc Jpn 91:091008
71. Arai Y, Paradis P-F, Aoyama T, Ishikawa T, Yoda S (2003) Rev Sci Instrum 74:1057
72. Hakamada S, Nakamura A, Watanabe M, Kargl F (2017) Int J Microgravity Sci Appl 34:340403
73. Langstaff D, Gunn M, Greaves GN, Marsing A, Kargl F (2013) Rev Sci Instrum 84, 124901
74. Nagashio K, Yamaguchi O, Hibiya T, Kuribayashi K (2006) J Am Ceram Soc 89:1504
75. Nagashio K, Kuribayashi K, Yamaguchi O, Hibiya T (2007) J Am Ceram Soc 90:238
76. Ushakov SV, Shvarev A, Alexeev T, Kapush D, Novrotsky A (2017) J Am Ceram Soc 100:754
77. Kondo T, Muta H, Ohishi Y (2021) High Temp High Press 50:35
78. Sun Y, Duan G, Yamaji A, Takatani T, Muta H, Ohishi Y (2022) npj Microgravity 8, 26
79. Weber JKR, Hampton DS, Merkley DR, Rey CA, Zatarski MM, Nordine PC (1994) Rev Sci Instrum 65:456
80. Nordine PC, Merkley D, Sickel J, Finkelman S, Telle R, Kaiser A, Prieler R (2012) Rev Sci Instrum 83:125107
81. Weber JKR, Felten JJ, Cho B, Nordine PC (1996) J Jpn Soc Microgravity Appl 13:27
82. Nagashio K, Takamura Y, Kuribayashi K, Shiohara Y (1999) J Cryst Growth 200:118
83. Nagashio K, Kuribayashi K, Takamura Y (2000) Acta Mater 48:3049
84. Nagashio K, Kuribayashi K (2001) Acta Mater 49:1947
85. Nagashio K, Kuribayashi K, Shiohara Y (2001) Acta Mater 49:2557
86. Li M, Nasgashio K, Kuribayashi K (2001) Scripta Mater 45:1431
87. Nagashio K, Kuribayashi K (2002) Acta Mater 50:1973
88. Nagashio K, Kuribayashi K (2002) J Am Ceram Soc 85:2550
89. Nagashio K, Kuribayashi K (2002) J Am Ceram Soc 85:2353
90. Li M, Nagashio K, Kuribayashi K (2002) Scripta Mater 47:213
91. Li M, Nagashio K, Kuribayashi K (2003) J Cryst Growth 249:625
92. Gustafson DE, Hofmeister WH, Bayuzick RJ, Nagashio K, Kuribayashi K (2003) Mater Sci Eng, A 341:1
93. Li M, Nagashio K, Kuribayashi K (2004) Mater Sci Eng A375–377:528
94. Li M, Nagashio K, Kuribayashi K (2003) Phil Mag 83:1095
95. Ushakov SV, Niessen J, Quirinale DG, Prieler R, Navrotsky A, Telle R (2021) Materials 14:822
96. Barbé J-C, Parayre C, Daniel M, Papoular M, Kernevez N (1999) Int J Thermophys 20:1071
97. Piluso P, Monerris J, Journeau C, Cognet G (2002) Int J Thermophys 23:1229
98. Grishchenko D, Piluso P (2011) High Temp High Press 40, 127
99. Sugioka K, Komori S (2007) J Fluid Mech 570:155
100. Hyers RW, Trapaga G, Abedian B (2003) Metall Mater Trans 34B:29
101. Xiao X, Brillo J, Lee J, Hyers RW, Matson DM (2021) npj Microgravity 7, 36
102. Rhim W-K, Chung SK, Barber D, Man KF, Gutt G, Rulison A, Spjut RE (1993) Rev Sci Instrum 64:2961
103. Ishikawa T, Paradis P-F, Itami T, Yoda S (2005) Meas Sci Technol 16:443
104. Paradis P-F, Ishikawa T, Lee GW, Holland-Moritz D, Brillo J, Rhim W-K, Okada JT (2014) Mater Sci Eng R 76:1
105. Chung SK, Thiessen DB, Rhim W-K (1996) Rev Sci Instrum 67:3175
106. Rhim W-K, Ohsaka K, Paradis P-F, Spjut RE (1999) Rev Sci Instrum 70:2796
107. Rulison AJ, Rhim W-K (1994) Rev Sci Instrum 65:695
108. Gangopadhyay AK, Lee GW, Kelton KF, Rogers JR, Goldman AI, Robinson DS, Rathz TJ, Hyers RW (2005) Rev Sci Instrum 76:073901
109. Masaki T, Ishikawa T, Paradis P-F, Yoda S, Okada JT, Watanabe Y, Nanao S, Ishikura A, Higuchi K, Mizuno A, Watanabe M, Kohara S (2007) Rev Sci Instrum 78:026102
110. Aoki H, Paradis P-F, Ishikawa T, Aoyama T, Masaki T, Yoda S (2003) Rev Sci Instrum 74:1147
111. Kordel T, Holland-Moritz D, Yang F, Peters J, Unruh T, Hansen T, Meyer A (2011) Phys Rev B 83:104205

112. Ryu CW, Dmowski W, Kelton KF, Lee GW, Park ES, Morris JR, Egami T (2019) Sci Rep 9:18579
113. Paradis P-F, Yu J, Ishikawa T, Aoyama T, Yoda S (2004) Appl Phys A 79:1965
114. Paradis P-F, Yu J, Aoyama T, Ishikawa T, Yoda S (2003) J Am Ceram Soc 86:2234
115. Paradis P-F, Yu J, Ishikawa T, Aoyama T, Yoda S, Weber JKR (2003) J Cryst Growth 249:523
116. Paradis P-F, Ishikawa T, Saita Y, Yoda S (2004) Jpn J Appl Phys 43:1496
117. Tamaru H, Koyama C, Saruwatari H, Nakamura Y, Ishikawa T, Takada T (2018) Microgravity Sci Technol 30:643
118. Zhang P, Zhang Y, Wang Z, Wang Y, Li M, Niu R, Yang W, Gao M, Zhong H, Li X, Yu J (2022) npj Microgravity 8, 29
119. Rhim W-K, Paradis P-F (1999) Rev Sci Instrum 70:4652
120. Le Maux D, Klapczynski V, Courtois M, Pierre T, Le Masson P (2022) J Mater Sci 57:12094
121. Rhim W-K, Ishikawa T (1998) Rev Sci Instrum 69:3628
122. Zhong Q, Yang L, Li H, Tao Y, Wang W, Xu Z, Luo C (2020) J Mol Liq 316:113345
123. Ishikawa T, Paradis P-F, Yoda S (2001) Rev Sci Instrum 72:2490
124. Gong Y, Zhang L, Yuan Y, Guo Q, Ma W, Huang S (2022) Front Energy Res 10:892406
125. Glorieux B, Millot F, Rifflet JC, Coutures J-P (1999) Int J Thermophys 20:1085
126. Coutures J-P, Rifflet J-C, Florian P, Massiot D (1994) Rev Int Hautes Temp Refract 29:123
127. Granier B, Heurtault S (1983) Rev Int Hautes Temp Refract 20:31
128. Zubarev YV, Kostikov VI, Mitin BS, Nagibin YA, Nischeta V (1969) Izv Akad Nauk SSSR Neorg Mat 5, 1563
129. Wartenberg HV, Wehner E, Saran E (1936) Nach Akad Wiss Goettingen 2:65
130. Kozakevitch P (1960) Rev Mater Paris 57:14
131. Kingery WD (1959) J Am Ceram Soc 42:6
132. Ikemiya N, Umemoto J, Hara S, Ogino K (1993) ISIJ Int 33:156
133. Shpil'rain EE, Yakimovich KA, Tsitsarkin AF (1973) High Temp High Press 5:191
134. Elyutin VP, Mitin BS, Anisimov YuS (1973) Neo Mater 9:1585
135. Mitin B, Nagibin YA (1970) Russ J Phys Chem 44:741
136. Kirshenbaum AD, Cahill JA (1960) J Inorg Nucl Chem 14:283
137. Rasmussen JJ, Nelson RPJ (1971) J Am Cram Soc 54:398
138. Granier B, Heurtault S (1998) J Am Ceram Soc 71:C466
139. Ishikawa T, Koyama C, Saruwatari H, Tamaru H, Oda H, Ohshio M, Nakamura Y, Watanabe Y, Nakata Y (2020) High Temp High Press 49:5
140. Koyama C, Ishikawa T, Oda H, Saruwatari H, Ueno S, Oshio M, Watanabe Y, Nakata Y (2021) J Am Ceram Soc 104:2913
141. Ishikawa T, Koyama C, Oda H, Shimonishi R, Ito T, Paradis P-F (2022) Metals 12:1126
142. Fyhrie M, Hong QJ, Kapush D, Ushakov SV, Liu H, van deWalle A, Navrotsky A (2019) J Chem Thermodyn 132, 405
143. Kondo T, Muta H, Kurosaki K, Kargl F, Yamaji A, Furuya M, Ohishi Y (2019) Heliyon 5:e02049
144. Hong Q-J, Ushakov SV, Kapush D, Benmore CJ, Weber RJK, van de Walle A, Navrotsky A (2018) Sci Rep 8:14962
145. Gallington L, Ghadar Y, Skinner LB, Weber JKR, Ushakov SV, Navrotsky A, Vazquez-Mayagoitia A, Neuefeind JC, Stan M, Low J, Benmore C (2017) Materials 10:1290
146. Rayleigh L (1879) Proc R Soc London 29:71
147. Lamb H (1932) Hydrodynamics, 6th ed. Cambridge University Press, Cambridge, p 473
148. Paradis P-F, Ishikawa T (2005) Jpn J Appl Phys 44:5082
149. Ishikawa T, Koyama C, Oda H, Saruwatari H, Paradis P-F (2022) Int J Microgravity Sci Appl 39:390101
150. Glorieux B, Saboungi M-L, Millot F, Enderby J, Rifflet J-C (2001) AIP Conf Proc 552:316
151. Maurakh MA, Mitin BS, Roitberg MB (1967) Zavod Lab 33:984
152. Lihrmann JM, Haggerty JS (1985) J Am Ceram Soc 68:81
153. Bartlett RM, Hall JK (1965) Ceramic Bull 44:444
154. McNally RN, Yeh HC, Balasubramanian N (1968) J Mater Sci 3:136

155. Elyutin VP, Mitin BS, Nagibin YA (1971) Zavod Lab 2:194
156. Anisimov YuS, Grifts EF, Mitin BS (1977) Izv Akad Nauk SSSR Neorg Mater 13:1444
157. Kondo T, Muta H, Ohishi Y (2020) J Nucl Sci Technol 57:889
158. Bates JL, McNeilly CE, Rasmussen JJ (2020) Material science research. In: Kriegel WW, Palmour H (eds), vol 5. Plenum Press, New-York, p 11
159. Bloomquist RA, Fink JK, Leibowitz L (1978) Am Ceram Soc Bull 57:522
160. Rossin R (1964) Rev Hautes Temp Refract 1:159
161. Urbain G (1982) Rev Int Hautes Tempér Réfract 19:55
162. Castanet R (1984) High Temp High Press 16:449
163. Kantor PB, Lazareva LS, Kandyba VV, Fomichov EM (1962) Ukr Fiz Zh 7:205
164. Sheindlin AE, Chekhovskoi VY, Petrov VA (1964) Inzh-Fiz Zh 7:63
165. Shpil'rain EE, Kagan DN, Barkhatov LS (1972) High Temp High Press 4, 605
166. Kapush D, Ushakov SV, Navrotsky A, Hong Q-J, Liu H, van de Walle A (2017) Acta Mater 124:204
167. Ushakov SV, Maram PS, Kapush D, Pavlik AJ III, Fyhrie M, Gallington LC, Benmore CJ, Weber R, Neuefeind JC, McMurray JW, Navrotsky A (2018) Adv Appl Ceram 117:S82
168. Ushakov SV, Navrotsky A (2011) J Mater Res 26:845
169. Navrotsky A, Ushakov SV (2017) Am Ceram Soc Bull 96, 22
170. Fyhrie M, Hong Q-J, Kapush D, Ushakov SV, Liu H, van de Walle A, Navrotsky A (2019) J Chem Thermodyn 132:405
171. Sun Y, Muta H, Ohishi Y (2021) Rev Sci Instrum 92:095102
172. Ranz WE, Marshall WR Jr (1952) Chem Eng Prog 48:141
173. Kim WK, Shim JH, Kaviany M (2017) J Nucl Mater 491:126
174. Masuno A, Arai Y, Yu J (2008) Phase Transit 81:553
175. Krishnan S, Anderson CD, Nordine PC (1994) Phys Rev B 49:3161
176. Pottlacher G, Boboridis K, Cagran C, Hüpf T, Seifter A, Wilthan B (2013) AIP Conf Proc 1552:704
177. Kobatake H, Kurokawa Y, Iwabuchi M, Adachi M, Ohotsuka M, Fukuyama H, Yamaguchi Y, Yamada Y, Sasajima N (2023) Meas Sci Technol 34:015010